
DIGITAL ACCESS TO SCHOLARSHIP AT HARVARD
DASH.HARVARD.EDU


HARVARD LIBRARY
Office for Scholarly Communication

Global chemical model analysis of biomass burning and lightning influences over the South Pacific in austral spring

Citation

Staudt, Amanda C., Daniel J. Jacob, Jennifer A. Logan, David Bachiochi, T. N. Krishnamurti, and Nathalie Poisson. 2002. "Global Chemical Model Analysis of Biomass Burning and Lightning Influences over the South Pacific in Austral Spring." Journal of Geophysical Research 107, issue D14: ACH 11-1-ACH 11-17.

Published Version

doi:10.1029/2000JD000296

Permanent link

http://nrs.harvard.edu/urn-3:HUL.InstRepos:14117816

Terms of Use

This article was downloaded from Harvard University's DASH repository, and is made available under the terms and conditions applicable to Other Posted Material, as set forth at http://nrs.harvard.edu/urn-3:HUL.InstRepos:dash.current.terms-of-use#LAA

Share Your Story

The Harvard community has made this article openly available.
Please share how this access benefits you. Submit a story .

Accessibility

JOURNAL OF GEOPHYSICAL RESEARCH, VOL. 107, NO. D14, 4200, 10.1029/2000JD000296, 2002

Global chemical model analysis of biomass burning and lightning influences over the South Pacific in austral spring

Amanda C. Staudt, Daniel J. Jacob, and Jennifer A. Logan

Division of Engineering and Applied Sciences and Department of Earth and Planetary Sciences, Harvard University, Cambridge, Massachusetts, USA

David Bachiochi and T. N. Krishnamurti

Department of Meteorology, Florida State University, Tallahassee, Florida, USA

Nathalie Poisson

Agence de l'Environnement et de la Maitrise de L'Energie, Paris, France

Received 27 December 2000; revised 18 July 2001; accepted 28 July 2001; published 20 July 2002.

[1] A global three-dimensional model of tropospheric chemistry driven by reanalyzed European Centre for Medium-Range Weather Forecasts meteorological data is used to examine the sources of O_3, CO, and nitrogen oxides (NO_x = NO + NO_2) in the South Pacific troposphere during the NASA Pacific Exploratory Mission to the Tropics (PEM-Tropics A) in September–October 1996. Aircraft observations up to 12 km during that mission revealed considerable biomass burning influence on O_3 and CO in terms of elevated pollution layers and regional enhancements. The model reproduces the long-range transport of biomass burning effluents from southern Africa and South America in the westerly subtropical flow over the South Pacific. Meteorological conditions in 1996 were particularly favorable for this transport. Africa and South America make comparable contributions to the biomass burning pollution over the South Pacific; the contribution from Australia and Indonesia is much less. Biomass burning dominates the supply of NO_x in the lower troposphere over the South Pacific (through long-range transport and decomposition of peroxyacetylnitrate), but lightning dominates in the upper troposphere. Observations in PEM-Tropics A and elsewhere indicate low HNO_3/NO_x concentration ratios and an imbalance in the chemical budget of NO_x in the upper troposphere. We reproduce these observations in our model and show that they reflect the subsidence of primary NO_x injected by lightning into the uppermost troposphere, rather than any fast chemistry recycling HNO_3 to NO_x. We find that biomass burning and lightning made similar contributions to O_3 production over the South Pacific during PEM-Tropics A. Biomass burning plumes sampled in PEM-Tropics A contained little NO_x, and the O_3 enhancements observed in these plumes originated from production over the source continents rather than over the South Pacific. *INDEX TERMS:* 0365 Atmospheric Composition and Structure: Troposphere—composition and chemistry; 0368 Atmospheric Composition and Structure: Troposphere—constituent transport and chemistry; 0345 Atmospheric Composition and Structure: Pollution—urban and regional (0305); 0322 Atmospheric Composition and Structure: Constituent sources and sinks; *KEYWORDS:* troposphere, pollution, PEM-Tropics, biomass burning, lightning, greenhouse

1. Introduction

[2] The Pacific Exploratory Mission to the Tropics (PEM-Tropics A) aircraft mission over the South Pacific in September–October 1996 (see Figure 1 for flight tracks) revealed ubiquitous biomass burning pollution plumes, typically a few kilometers in vertical extent and hundreds of kilometers in north-south extent [*Hoell et al.*, 1999]. This finding demonstrated that biomass burning, which is maximum in the austral tropics during the July–November dry season [e.g., *Hao and Liu*, 1994], influences the most remote regions of the tropical troposphere. Of concern is how chemical reactions involving biomass burning effluents in the tropical troposphere affect concentrations of ozone (O_3), a greenhouse gas, and of the hydroxyl radical (OH), the main atmospheric oxidant, relative to natural conditions where emissions from lightning and the biosphere dominate the chemistry. In this paper, we use a global three-dimensional (3-D) chemical transport model driven by assimilated meteorological observations to examine the origins of biomass burning pollution plumes observed in PEM-Tropics A and to assess their effect on the chemistry of the Pacific troposphere.

Copyright 2002 by the American Geophysical Union.
0148-0227/02/2000JD000296

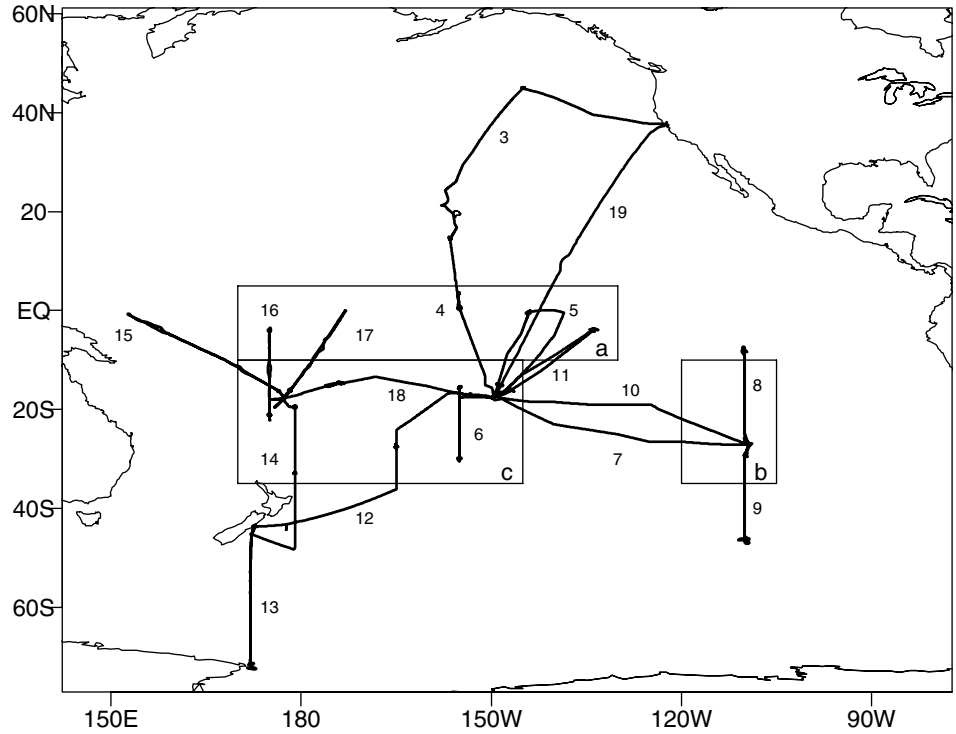

Figure 1. Map of PEM-Tropics A flight tracks for the DC-8 aircraft. Observations from PEM-Tropics A are averaged over three regions for model evaluation: Equatorial South Pacific (boxed area a), Eastern South Pacific (boxed area b), and Subtropical South Pacific (boxed area c).

[3] The biomass burning plumes were characterized by elevated O_3, carbon monoxide (CO), hydrocarbons, peroxyacetylnitrate (PAN), and methyl halides combined with low relative humidity and tetracholoroethene (C_2Cl_4) [*Blake et al.*, 1999]. *Dibb et al.* [1999a] concluded that the biomass burning plumes had been convectively processed near their source region because they were depleted in biomass burning aerosol tracers such as elemental C, NH_4^+, and K^+ and then did not experience subsequent scavenging during transport because they had elevated ^{210}Pb, a decay product of ^{222}Rn which attaches to aerosols. Elevated concentrations of nitric acid (HNO_3) and hydrogen peroxide (H_2O_2), which are also removed efficiently by wet scavenging, confirm that the plumes had not recently experienced convection and had traveled long enough for significant photochemical processing [*Dibb et al.*, 1999b; *Cohan et al.*, 1999]. Thus the typical plume formed when continental air polluted by biomass burning was convected to the upper troposphere and then carried long distances during which it experienced subsidence and additional photochemical activity [*Schultz et al.*, 1999]. Hydrocarbon concentration ratios measured in the plumes implied a transport time of 1–2 weeks from the point of emission [*Blake et al.*, 1999; *Dibb et al.*, 1999b]. Back trajectories computed along the flight tracks by *Board et al.* [1999] show that most plumes were transported to the South Pacific by strong westerly winds at subtropical latitudes. The trajectories extend back to southern Africa or South America within 10 days, consistent with the photochemical age estimates.

[4] Southern Africa and Brazil are the two dominant biomass burning source regions of the austral tropics [*Hao and Liu*, 1994]. The Transport and Atmospheric Chemistry Near the Equator—Atlantic (TRACE-A) aircraft mission, conducted in September–October 1992 over these source regions and the South Atlantic [*Fishman et al.*, 1996a], provided considerable information on the composition and near-field transport of biomass burning pollution. *Thompson et al.* [1996] found that South American pollution is frequently convected to the upper troposphere and then advected across the South Atlantic, while African pollution is transported below 4–5 km toward the South Atlantic in the prevailing easterlies. The air above the South Atlantic slowly recirculates around a semipermanent center of high pressure [*Krishnamurti et al.*, 1993] allowing for the formation of an O_3 maximum observable from satellites [*Fishman et al.*, 1996b]. Some southern African pollution is exported southeastward to the Indian Ocean where it can accumulate by circulation around the semipermanent Mascarene High situated above Madagascar [*Garstang et al.*, 1996; *Tyson et al.*, 1996]. Air is episodically flushed from these accumulation regions by westerly moving midlatitude frontal systems [*Diab et al.*, 1996; *Chatfield et al.*, 1998]. In this paper, we will show that this flushing played a major role in the formation of the biomass burning plumes observed over the South Pacific during PEM-Tropics A.

[5] The large-scale distribution of chemical species over the South Pacific was clearly affected by biomass burning outflow. Pollutants observed during PEM-Tropics A show a strong longitudinal gradient across the South Pacific with elevated concentrations at 2–8 km in the western Pacific troposphere [*Blake et al.*, 1999; *Singh et al.*, 2000]. The South Pacific Convergence Zone (SPCZ), which stretched along a northwest–southeast axis from 140°E at the equator to 150°W at 20°S [*Fuelberg et al.*, 1999], was an effective

barrier for horizontal mixing; significantly higher median concentrations of biomass burning tracers were observed to the south of the SPCZ compared to the north [*Gregory et al.*, 1999; *Talbot et al.*, 1999]. Thus the equatorial South Pacific troposphere (0°–10°S) exhibited little biomass burning influence, while air to the south had considerably more [*Fenn et al.*, 1999; *Gregory et al.*, 1999; *Schultz et al.*, 1999].

[6] Relatively little attention has been paid to photochemical production of O_3 in the aged biomass burning plumes sampled in PEM-Tropics A. On the basis of calculations with a local photochemical model as well as with a global 3-D model driven by general circulation model (GCM) meteorology, *Schultz et al.* [1999] concluded that half of the O_3 observed in the 0–12 km column over the South Pacific during PEM-Tropics A was photochemically produced within the region at a rate limited by the supply of nitrogen oxide radicals (NO_x = NO + NO_2) in the plumes and in the large-scale atmosphere where the plumes disperse. The other half was transported into the region and included a dominant contribution from biomass burning. Although biomass burning is a large source of NO_x, the lifetime of NO_x against oxidation is short (ranging from <1 day in the lower troposphere to ~10 days in the upper troposphere), so that chemical recycling of NO_x from its reservoir species HNO_3 and PAN is necessary to sustain NO_x levels sufficient for continued O_3 production. Observed NO concentrations were generally low over the South Pacific, ranging from a few parts per trillion by volume (pptv) near the surface to 50–150 pptv in the upper troposphere. However, on the basis of local photochemical model calculations, *Schultz et al.* [2000] concluded that chemical recycling from the HNO_3 and PAN reservoirs could not account for the observed NO_x levels. Previous studies of the NO_x budget in other regions of the free troposphere have found a similar imbalance between chemical sources and sinks; fast heterogeneous conversion from HNO_3 to NO_x on sulfate aerosols [*Chatfield*, 1994; *Fan et al.*, 1994] or on soot [*Hauglustaine et al.*, 1996; *Lary et al.*, 1997] has been proposed as an explanation. At this point, there is no experimental support for such fast heterogeneous reactions of HNO_3 [*Jacob*, 2000].

[7] Although techniques such as back trajectories, the age of air, and local photochemical modeling can give a general idea about the origin of biomass burning pollution over the South Pacific and its chemical evolution, a 3-D model can better resolve the coupling between transport, convection, and photochemistry. We have interfaced the Harvard chemical tracer model with assimilated meteorological data from the Florida State University (FSU) global spectral model to create a global 3-D model of atmospheric chemistry and transport for the PEM-Tropics A period. The Harvard/FSU model is better suited to studies of the PEM-Tropics A data than the 3-D GCM-based model used by *Schultz et al.* [1999] because it simulates actual dynamical conditions for the period of observations and has an improved treatment of tropical dynamics. We use the model to investigate the origins of the biomass burning pollution plumes sampled during PEM-Tropics A, to examine how dispersal of biomass burning pollution modifies NO_x and O_3 concentrations over the South Pacific on a larger scale, and to compare the roles of biomass burning and lightning in that context.

[8] The Harvard/FSU model is described in section 2, followed by a model evaluation with PEM-Tropics A observations in section 3. The mechanisms for long-range transport of biomass burning plumes over the South Pacific are examined in section 4, and the contribution of each source region to the biomass burning pollution in the Southern Hemisphere is quantified. The factors which affect the budgets of NO_x and O_3 over the South Pacific are addressed in sections 5 and 6, respectively. Conclusions are offered in section 7.

2. Harvard/FSU Chemical Transport Model Description

[9] We have interfaced the Harvard chemical transport model (CTM) for O_3-NO_x-hydrocarbon chemistry [*Wang et al.*, 1998; *Horowitz and Jacob*, 1999; *Bey et al.*, 2001a] with assimilated meteorological fields produced by FSU for July 22 through October 6, 1996. The FSU model has been used for many applications, including hurricane tracks [*Krishnamurti et al.*, 1989] and passive tracer studies investigating transport in the South Atlantic region [*Krishnamurti et al.*, 1993, 1996]. An emphasis on accurately simulating tropical dynamics during the period of the PEM-Tropics A mission makes the FSU assimilated meteorological fields particularly well suited for our application. In particular, the precipitation rates used in the physical initialization procedure are derived from satellite observations of outgoing longwave radiation and precipitation [*Krishnamurti et al.*, 1983; *Gairola and Krishnamurti*, 1992]. The CTM has a horizontal resolution of 4° latitude by 5° longitude and 14 sigma vertical levels centered at 0.99, 0.95, 0.9, 0.85, 0.8, 0.7, 0.6, 0.5, 0.4, 0.3, 0.2, 0.1, 0.07, and 0.03; the model top is at 10-hPa altitude.

[10] Tracer advection is simulated with a second-order moments scheme [*Prather*, 1986]. Mixing of air and tracers by dry and wet convection is parameterized mostly following the approach of *Wild and Prather* [2000]. For dry convection the Harvard/FSU model redistributes tracer mass uniformly over all layers and fractions of layers up to the local mixed layer height. Wet convection is driven by subgrid convective vertical velocities supplied by FSU. These velocities are converted to fluxes using a convective cloud area which is parameterized as a function of grid-scale convective precipitation following *Slingo* [1987]. Starting at the bottom of each column, if there is a net upwards cloud mass flux out of a grid box, the amount of air that must be moved out of the box to conserve mass balance is entrained into a "pipe" and carried upward to the next grid box. If the upward convective mass flux through the top of this next grid box is greater than the flux through the bottom, then the air already in the convective pipe is preserved and additional air is entrained into the pipe to reflect the convective mass flux convergence; the air in the pipe is transported upward to the next grid box and the process is repeated. When the pipe encounters a grid box where the convective mass flux through the top is less than through the bottom, then it is partly or totally detrained into that grid box. Compensatory large-scale subsidence outside the pipe allows the grid column to retain its original air mass distribution so that convection results in no net transport of air mass.

Table 1. Global Emissions for CO and NO_x (August 28 through October 6, 1996)

	Southern Hemisphere	Northern Hemisphere
	CO (Tg CO)	
Fossil fuel combustion	2.1 (3%)	38 (60%)
Biofuel	2.9 (4%)	11 (18%)
Biomass burning	63 (93%)	14 (22%)
South America	29	1.2
Africa	26	8.8
Indonesia/Australia	8.0	3.5
	NO_x (Tg N)	
Fossil fuel combustion	0.3 (6%)	3.9 (65%)
Biomass burning	2.9 (71%)	0.6 (10%)
Soil	0.3 (8%)	0.6 (10%)
Lightning	0.6 (15%)	0.8 (14%)
Aircraft	0.004 (<1%)	0.06 (1%)

[11] The Harvard chemistry, deposition, and emissions schemes [*Wang et al.*, 1998; *Horowitz and Jacob*, 1999] are employed in this new model with only a few adaptations. Eighty species, including 24 transported tracers, are included to represent tropospheric O_3-NO_x-hydrocarbon chemistry. The chemical mechanism is that of *Horowitz et al.* [1998], with minor updates as discussed by *Bey et al.* [2001a], and is integrated with a fast Gear solver [*Jacobson and Turco*, 1994]. The reaction rates for HNO_3 + OH and for NO_2 + OH are from work by *Portmann et al.* [1999]. Heterogeneous chemistry follows the recommendations of *Jacob* [2000], using a monthly mean sulfate aerosol field calculated by *Chin et al.* [1996], which is assumed to be wet or dry depending on the relative humidity. The mean aerosol surface area in the model over the South Pacific is 0.7 μm^2 cm^{-3}. Photolysis rates are computed with the Fast-J code of *Wild et al.* [2000], which includes accurate radiative transfer through clouds. Dry deposition of O_3, HNO_3, NO_2, CH_2O, H_2O_2, PAN, and other organic nitrates is calculated as described by *Jacob et al.* [1993]. Wet deposition of soluble tracers (HNO_3 and H_2O_2) is performed using the method developed by *Balkanski et al.* [1993]. A scavenging efficiency of 40% km^{-1} in wet convective updrafts, as recommended by *Liu et al.* [2001], is employed.

[12] Emissions of anthropogenic and biogenic NO_x, CO, and nonmethane hydrocarbons (NMHCs) are mostly as described by *Wang et al.* [1998]. Table 1 shows the emissions during the PEM-Tropics A time period (August 28 through October 5, 1996) for NO_x and CO. Emissions of NO_x from lightning (Figure 2) are parameterized as a function of the observed cloud top height, following *Price and Rind* [1992], and are distributed vertically with maximum concentrations in the upper troposphere and near the surface, following *Pickering et al.* [1998]. They are adjusted to yield a global source of 6 Tg N yr^{-1}, which provides the best simulation of NO, HNO_3, and O_3 as compared to the PEM-Tropics A observations. The accepted range for the global source of NO_x from lightning is 1–12 Tg N yr^{-1} [*Huntrieser et al.*, 1998]. Analyses of fire counts observed by satellite indicate that emissions during September 1996 were not substantially different from the long-term mean [*Olson et al.*, 1999]. We therefore use the climatological biomass burning emissions described by *Wang et al.* [1998], with minor adjustments in the spatial distribution of emissions over Africa and Australia to reflect the location of fires during September 1996 [*Olson et al.*, 1999]. The distribution of biomass burning emissions is shown in Figure 2 for NO_x.

[13] The fluxes from the stratosphere of O_3, NO_x, and HNO_3 contribute to the budgets of these species in the troposphere. The FSU model does not have the vertical resolution needed for an accurate simulation of stratospheric dynamics. We therefore use a cross-tropopause flux boundary condition for O_3 at 100 hPa altitude as described by *Wang et al.* [1998] with an annual global flux of 400 Tg yr^{-1} distributed by latitude and month of the year. We also use a flux of 0.48 Tg N yr^{-1} of NO_y computed by *Wang et al.* [1998] which is transported across the tropopause as NO_x and HNO_3 with a molar ratio of 1:4.

[14] The Harvard/FSU model is initialized in mid-July with chemical tracer fields produced by the Harvard/God-

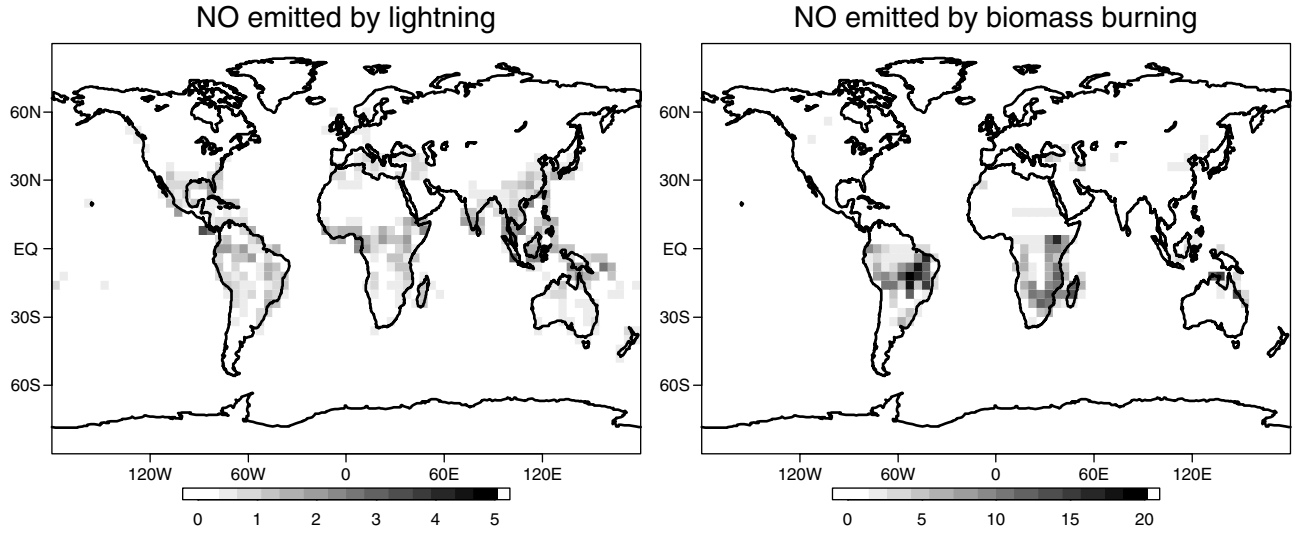

Figure 2. Distribution of NO_x emissions (1×10^{-10} molecules cm^{-2} s^{-1}) during the PEM-Tropics A time period (August 28 through October 5, 1996) from (left) lightning and (right) biomass burning.

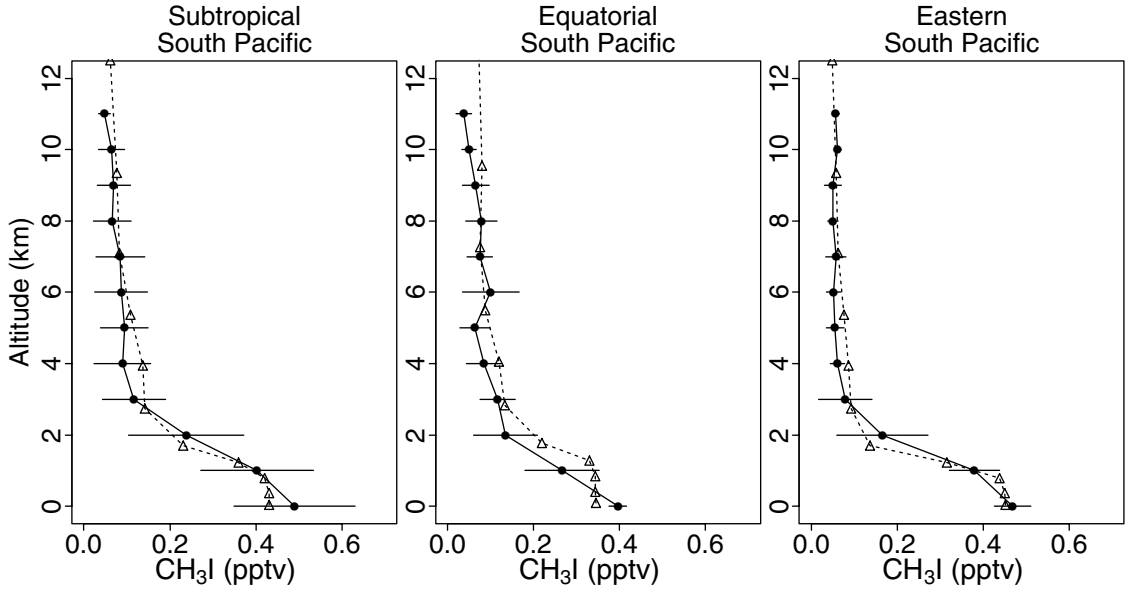

Figure 3. Comparison of simulated (dashed line) and observed (solid line) profiles of CH_3I concentrations over the South Pacific during PEM-Tropics A. Observations have been averaged over the regions identified in Figure 1. Error bars indicate ±1 standard deviation.

dard Institute for Space Studies (GISS) II chemical transport model [*Horowitz and Jacob*, 1999] for all species except O_3, which is initialized with observed tropospheric climatological values for July as prepared by *Logan* [1999]. The model is allowed to run for 6 weeks before the output is examined. This time period is sufficiently long to initialize transport patterns in the model.

3. Evaluation of General Model Features

3.1. Tracers of Vertical Transport

[15] Horizontal transport is generally well described in GCMs which use assimilated meteorological observations, but vertical transport is more difficult to capture because it must be inferred from a convergence of the horizontal winds and it includes a major contribution from subgrid convection. Simulation of long-range transport of biomass burning pollution in our model depends critically upon vertical transport both over land, where emitted gases are vented to the free troposphere, and over oceans, where these gases subside. We evaluated the representation of vertical transport in the Harvard/FSU model with simulations of ^{222}Rn to test continental convection and with simulations of CH_3I to test marine convection.

[16] Radon-222 is emitted from soils and decays radioactively with a lifetime of 5.5 days, making it useful as a tracer of continental convection [*Jacob and Prather*, 1990; *Mahowald et al.*, 1995]. The ^{222}Rn concentrations simulated by the model (not shown) compare favorably with the zonal mean and upper tropospheric concentrations presented in a recent intercomparison of global 3-D models [*Jacob et al.*, 1997]. In particular, concentrations of $\sim 20 \times 10^{-21}$ mol mol^{-1} are simulated at 300 hPa over the tropical continents, indicating rapid transport from the boundary layer to the upper troposphere. Despite ventilating the boundary layer well, continental convection in the Harvard/FSU model tends to distribute tracer through the column such that concentrations decrease monotonically from the surface, rather than showing a "C" profile with enhanced concentrations in the upper troposphere. This tendency of convection to create a well-mixed column is problematic for simulating distinct biomass burning plumes in the model and suggests that the model has insufficient convective outflow to the uppermost troposphere.

[17] Marine convection in the model was evaluated with CH_3I, a species with large oceanic emissions. Measurements of CH_3I concentrations were made by *Blake et al.* [1999] during PEM- Tropics A. Atmospheric loss of CH_3I is by photolysis with a lifetime of ~4 days in the tropics [*Cohan et al.*, 1999]. CH_3I provides a good test of marine boundary layer (MBL) venting because its ocean source is fairly uniform, its lifetime is short, and its loss process is simple and well defined. The MBL concentration of CH_3I, constrained by observations compiled by *Hsu et al.* [1999], is specified as a boundary condition in the lowest layer of the model (0–240 m). Photolysis rate constants are calculated using absorption cross-section data from *Roehl et al.* [1997]. Figure 3 compares calculated and observed vertical profiles of CH_3I during PEM-Tropics A. The model simulates successfully the MBL depth, the sharp concentration gradient between the MBL and the free troposphere, and the lack of a mean vertical gradient at higher altitudes which indicates that convective outflow is distributed vertically throughout the free troposphere. We conclude that MBL ventilation and marine convection are well reproduced in the model within the constraints afforded by CH_3I.

3.2. Evaluation of Full Chemistry Simulation

[18] Figure 4 shows comparison of the simulated concentrations with the PEM-Tropics A observations averaged over the regions in Figure 1. The simulated profiles are plotted as regional means (short-dashed lines with triangles) and as the mean concentration sampled along the flight tracks in each region and for the specific flight days (long-

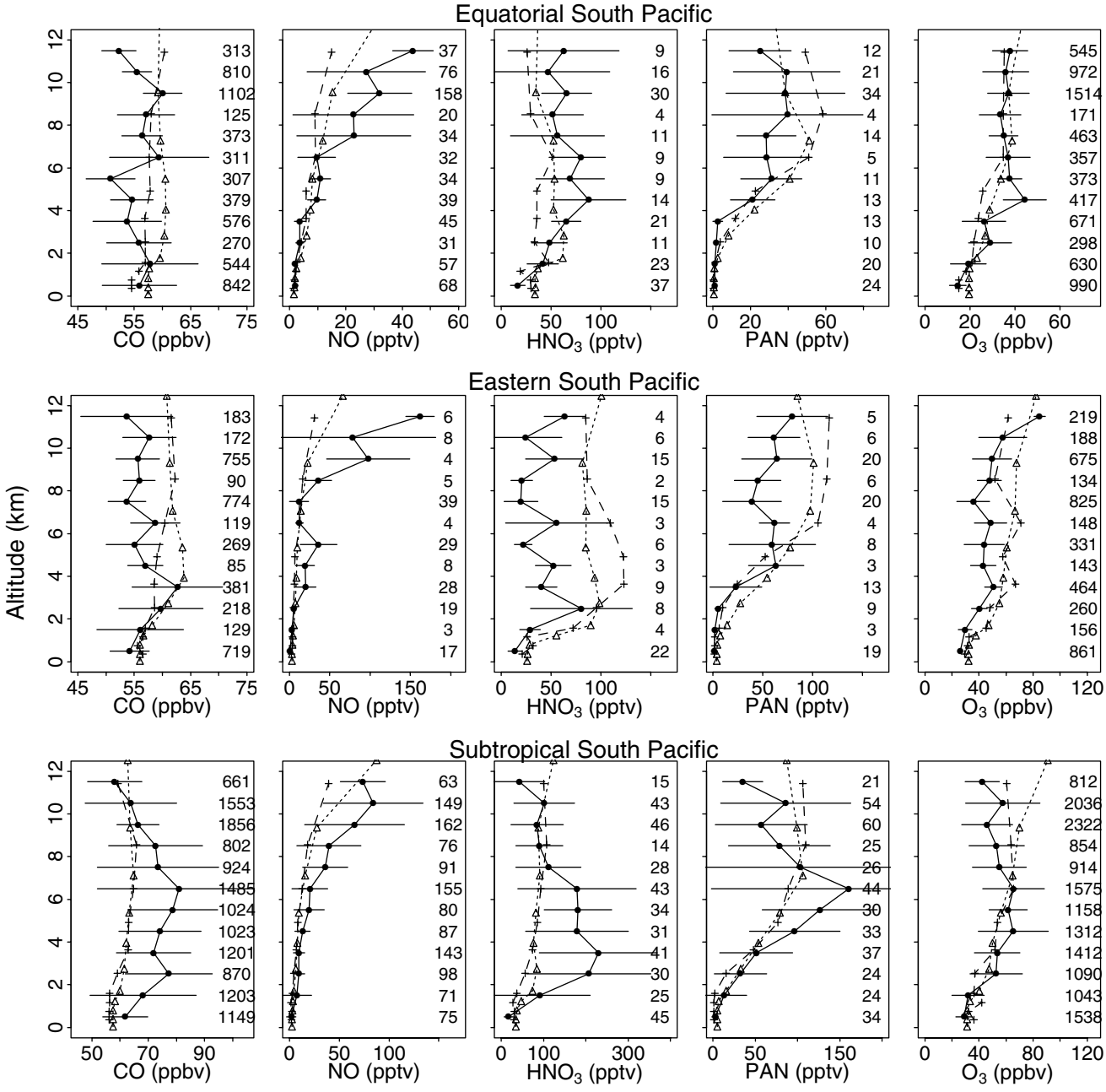

Figure 4. Comparison of simulated (short-dashed line with triangles) and observed (solid line) vertical profiles of CO, NO, HNO_3, PAN, and O_3 averaged over the PEM-Tropics A period (August 28 through October 5, 1996) and the regions identified in Figure 1. Error bars indicate ±1 standard deviation. Long-dashed line with crosses is the average of model values sampled along the flight tracks and for the flight days. Number of observations in each vertical interval is indicated on the right of each plot.

dashed lines with crosses). Simulated and observed scatterplots of O_3 versus CO are shown in Figure 5 for the middle troposphere over the South Pacific. Although two aircraft were used during PEM-Tropics A (the DC-8 and the P3-B), we focus our model evaluation on the DC-8 because it surveyed a larger domain, it had a higher ceiling (12 km altitude), and its suite of observations included HNO_3 and PAN. In addition to the aircraft observations, O_3 was measured by sondes launched from Samoa, Tahiti, and Easter Island on several days during the PEM-Tropics A mission. The model results are compared to the mean O_3 concentrations observed by sondes during September 1996 in Figure 6.

3.2.1. Carbon Monoxide

[19] Carbon monoxide concentrations observed over the equatorial South Pacific during PEM-Tropics A ranged between 50 and 60 ppbv with little vertical gradient and small standard deviations (Figure 4). The model reproduces these low concentrations and the lack of variability in this region, which contains well-aged and well-mixed air. Observed CO concentrations over the eastern South Pacific are also ~50–60 ppbv throughout the column except for an

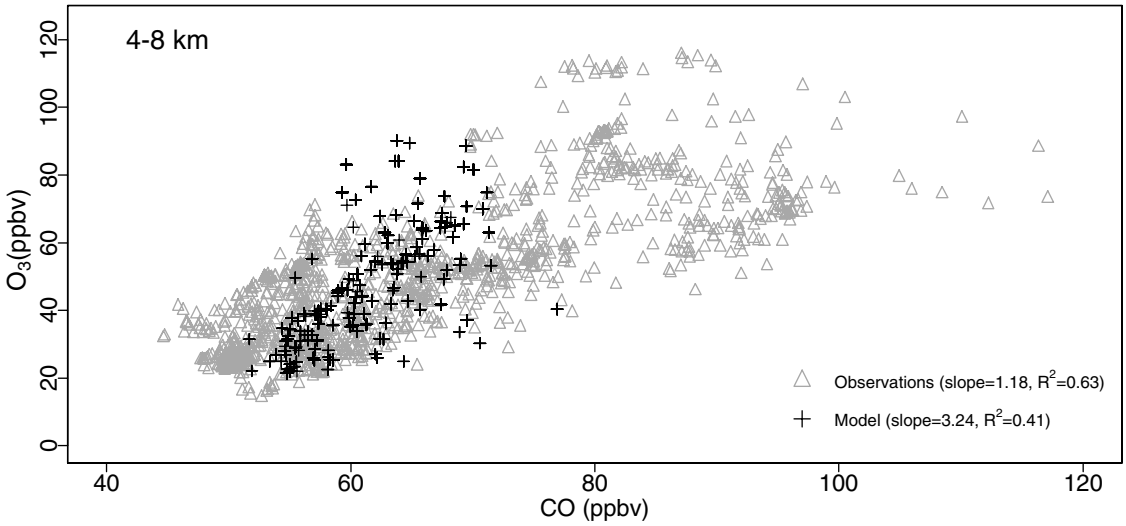

Figure 5. Scatterplot of O_3 versus CO concentrations as observed on the DC-8 during PEM-Tropics A (triangles) and as sampled along the flight tracks in the Harvard/FSU model (crosses) for a South Pacific region extending from 0°–25°S, 165°E–105°W, and 4–8 km altitude.

enhancement around 3 km altitude due to biomass burning outflow directly from South America over the Pacific [*Blake et al.*, 1999; J. A. Logan et al., The origin and characteristics of biomass burning plumes observed over the Pacific Ocean during PEM-Tropics A, manuscript in preparation, 2000, hereinafter referred to as Logan et al., manuscript in preparation, 2000]. The model overestimates CO, HNO_3, PAN, and O_3 above the eastern South Pacific region, suggesting that the outflow from South America is distributed throughout the tropospheric above 3 km altitude in the model. The blocking effect of the Andes on the flow may not be fully reproduced. Unfortunately, only DC-8 flight 8, which flew north out of Easter Island, sampled this region. The observed CO distribution is therefore not well characterized.

[20] Above the subtropical South Pacific, westerly transport of biomass burning pollution from Africa and South America causes observed CO concentrations to be elevated and more variable [*Fuelberg et al.*, 1999; *Schultz et al.*, 1999; *Blake et al.*, 1999]. Although the simulated concentrations over the subtropical South Pacific are ~5 ppbv higher than those over the equatorial South Pacific, the model still underestimates the observed concentrations in the midtropospheric region impacted by biomass burning plumes (Figure 4). The model underestimate reflects an observational strategy biased toward sampling plumes and an inability of the model to reproduce the extreme concentrations observed in the plumes, as illustrated in Figure 5. Simulated CO concentrations rarely exceed 70 ppbv, while the observations extend up to 120 ppbv. We attribute the model underestimate of CO in biomass burning plumes over the Pacific to the tendency of convective transport over the tropical continents to create a well-mixed column rather

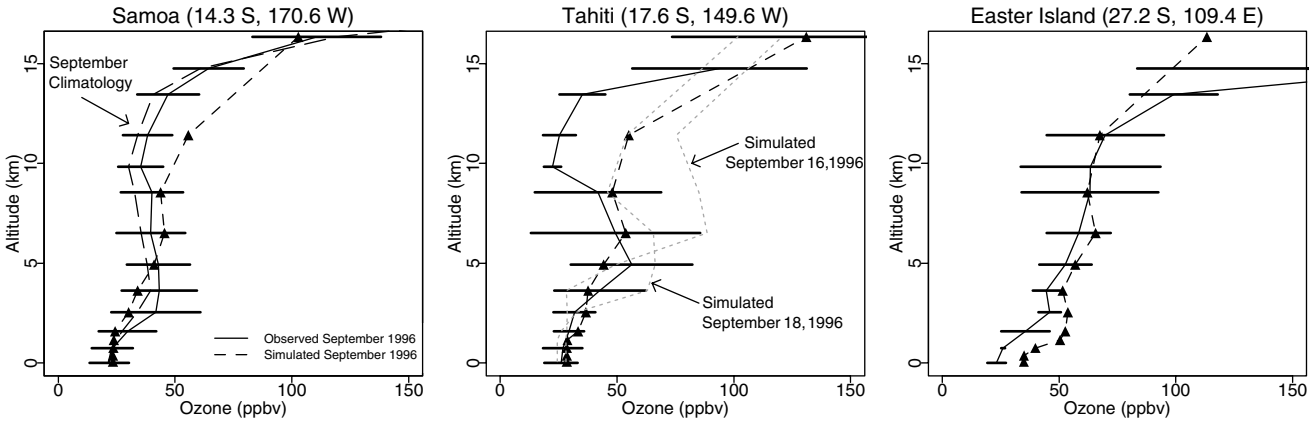

Figure 6. Ozone concentration vertical profiles above Samoa, Tahiti, and Easter Island during PEM-Tropics A. Solid line shows the mean values from O_3 sondes launched over the course of the PEM-Tropics A campaign, with error bars indicating ±1 standard deviation. Long-dashed lines are mean values from O_3 sondes launched at Samoa in September during 1986–1990 and 1995–1999. Short-dashed line with symbols is the mean simulated profile at the same location. Dotted lines in middle plot are model profiles for the days on which O_3 sondes were launched.

than layers of outflow confined to a few kilometers extent in the middle to upper troposphere, as discussed in section 3.1. Biomass burning pollution travelling at lower altitudes will take longer to reach the South Pacific, allowing more CO destruction during transit.

[21] The underestimate of CO in biomass burning plumes does not appear to reflect an inability of the model to maintain the vertical structure of the plumes during horizontal transport. In model experiments with a passive tracer artificially inserted in a narrow altitude band over southern Africa the vertical structure was preserved during the 1–2 weeks of tracer transport to the South Pacific. The *Prather* [1986] advection algorithm used here is known to be successful in preserving strong gradients with little numerical diffusion. The problem also does not appear to reflect an underestimate of biomass burning emissions. Doubling these emissions in the model increases CO concentrations above the subtropical South Pacific by 5–8 ppbv throughout the column but still does not reproduce the midtropospheric bulge. Increased biomass burning emissions also cause or aggravate overestimates of CO and O_3 above the eastern South Pacific.

3.2.2. Nitrogen Oxides, HNO_3, and PAN

[22] Concentrations of nitrogen oxides observed during PEM-Tropics A increase from the surface, where NO was as low as 1–2 pptv, to the upper troposphere, where NO was present at levels >50 pptv. The model reproduces the low NO observations in the MBL but tends to underestimate NO concentrations in the upper troposphere over all three of the South Pacific regions (Figure 4). Simulated NO concentrations in the upper troposphere over South America and Africa of 100–150 pptv are also low as compared to TRACE-A observations [*Pickering et al.*, 1996], suggesting that the model underestimates the injection of NO_x into the tropical upper troposphere by lightning. However, simple scaling of the lightning source causes the model to overestimate both HNO_3 and O_3 concentrations observed in PEM-Tropics A. A more likely explanation is that the FSU meteorological fields underestimate the frequency of very deep convective events discharging lightning NO_x to the uppermost troposphere. As we will see below, this explanation would also account for the model overestimate of O_3 in the upper troposphere.

[23] Observed HNO_3 concentrations are minimum over the equatorial South Pacific because of frequent scavenging associated with the Intertropical Convergence Zone (ITCZ). Likewise, convective mixing between the MBL, where PAN quickly thermally decomposes, and the upper troposphere depletes PAN throughout the column above the equatorial South Pacific. The model successfully reproduces the impact of convection on these two species. For the eastern South Pacific region the model overestimates free tropospheric HNO_3 and PAN concentrations, probably due to easterly export of biomass burning pollution from South America in the model, as was discussed previously for CO. Also similar to CO, the model underestimates midtropospheric concentrations of HNO_3 and PAN over the subtropical South Pacific region, where numerous plumes were sampled by the aircraft (Figure 4).

3.2.3. Ozone

[24] The aircraft observations during PEM-Tropics A show a gradient of increasing concentrations from the equatorial South Pacific, where free tropospheric concentrations average ~40 ppbv, to the subtropical South Pacific, where the mean free tropospheric concentrations are closer to 60 ppbv (Figure 4). The model captures this latitudinal gradient. Excessive easterly outflow of biomass burning pollution from South America is probably responsible for the model overestimate of aircraft observations of O_3 over the eastern South Pacific (Figure 4) and of the mean sonde observations at Easter Island (Figure 6). The model has more success simulating the observed midtropospheric bulge of O_3 concentrations over the subtropical South Pacific than it did for CO (Figures 4 and 5). This midtropospheric bulge is also apparent in the sonde observations over Tahiti and in the corresponding model profile (Figure 6). The high extremes in the CO observations are more muted for O_3, presumably because of the strong nonlinearity in net O_3 production [*Lin et al.*, 1988].

[25] The vertical distribution of O_3 concentrations over the South Pacific is in general consistent with observations, as shown in Figures 4 and 6. The most prominent discrepancy is an inability to capture the very low concentrations observed at 10–15 km altitude over Tahiti and to a lesser extent over Samoa. These low values must represent deep convective injection of boundary layer air, with detrainment above the ceiling of the aircraft; there is some indication of a decrease of O_3 concentrations at the highest altitudes in the aircraft observations over the subtropical South Pacific (Figure 4), but it is far less pronounced than in the sonde data. Insufficient transport into the uppermost troposphere during deep convection in the model could also be a major factor behind the underestimate of NO_x concentrations and of the NO_x/HNO_3 concentration ratio, as discussed further in section 5.

[26] An ubiquitous biomass burning influence on O_3 over the South Pacific during PEM-Tropics A is apparent in the correlation observed between O_3 and CO in the ensemble of the observations (Figure 5). At 4–8 km the two species are strongly correlated (R^2 = 0.63) with a slope of 1.2 mol mol^{-1}, consistent with biomass burning plumes over a week old [*Mauzerall et al.*, 1998]. Considering the remoteness from sources, the coherence of this relationship, as well as that between CO and other tracers of continental influence [*Blake et al.*, 1999], is remarkable. The model reproduces the positive correlation between O_3 and CO in the midtroposphere (slope = 3.2 mol mol^{-1}, R^2 = 0.41). The slope is higher in the model, which does not capture the relatively low $\Delta O_3/\Delta CO$ enhancement ratios observed in the strongest plumes.

4. Origin of Biomass Burning Plumes

4.1. Case Study for the September 18, 1996, Plume

[27] The Harvard/FSU model simulates several events of westerly outflow from southern Africa and South America which lead to elevated CO and O_3 in the tropical South Pacific troposphere. We show here one example of a model plume which was observed on September 18, 1996, by the DC-8 aircraft on flight 12 as it flew from Tahiti to Christchurch, New Zealand, and by an O_3 sonde launched from Tahiti (Figure 6) on the same day. Ozone concentrations of 60–80 ppbv, and occasionally higher, were observed in the midtroposphere for nearly the entire flight.

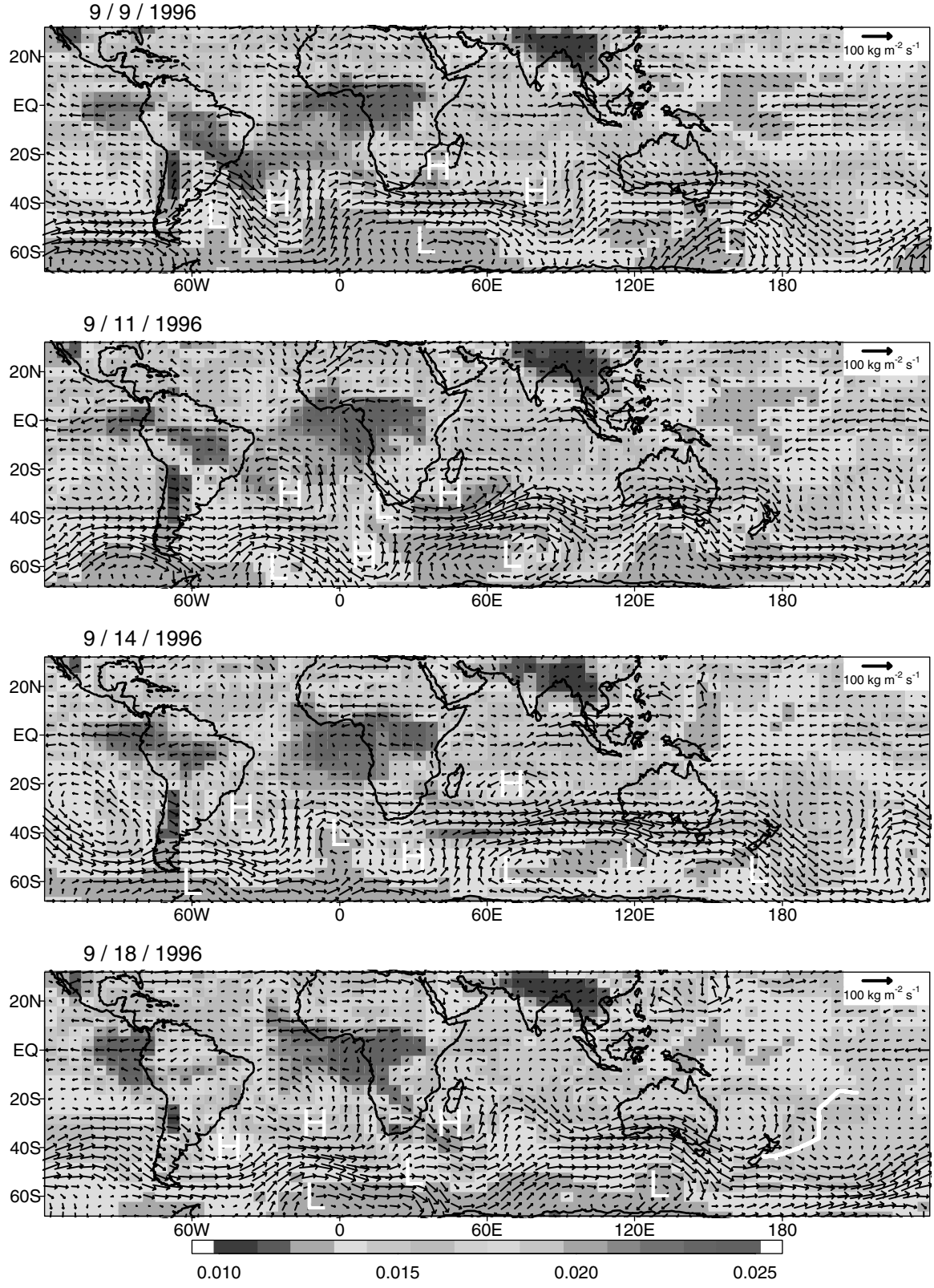

Figure 7. Simulated column CO above the boundary layer (700–85 hPa) in mol m^{-2} for 4 days leading up to the large biomass burning plume event observed between Tahiti and Christchurch, New Zealand, on September 18, 1996. Also shown are the corresponding daily mean centers of high and low surface pressure and air mass flux vectors at 500 hPa. See color version of this figure at back of this issue.

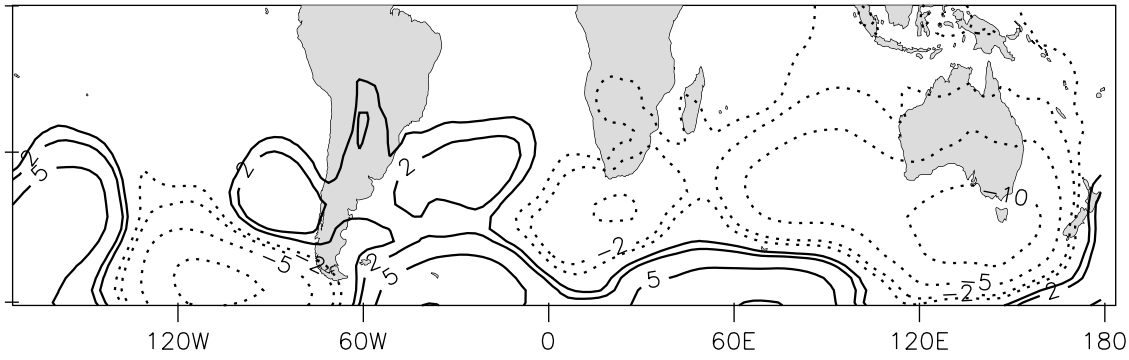

Figure 8. Mean pressure anomaly (hPa) for September 1996 relative to a 1958–1999 climatology from the NOAA National Centers for Environmental Protection/NCAR reanalysis.

Profiles of other species measured during ascents and descents of the plane confirmed the biomass burning origin of the elevated O_3 (enhanced CO and ethane, no C_2Cl_4 enhancement).

[28] The transport history of the September 18 plume is depicted in Figure 7, which shows the evolution of the free tropospheric CO column in the model for the September 9–18 period. Column abundances allow us to follow the plume even as it spreads or meanders vertically. Superimposed are the locations of high- and low-pressure centers and the mean horizontal air mass fluxes at 500 hPa, the altitude of maximum outflow from southern Africa to the Indian Ocean.

[29] On September 9, strong South American outflow to the South Atlantic was induced by a midlatitude cyclone located at 50°W and 45°S, just southwest of the subtropical South Atlantic High. Meanwhile, African biomass burning pollution was exported westward to the Atlantic free troposphere, as was documented extensively in TRACE-A [*Thompson et al.*, 1996; *Mauzerall et al.*, 1998; *Chatfield et al.*, 1998], as well as eastward to the Indian Ocean near the Mascarene High [*Garstang et al.*, 1996; *Tyson et al.*, 1996]. By September 11 a cut-off low, located southwest of the Mascarene High, enhanced the eastward outflow from Africa. On September 12, the Mascarene High shifted northeastward while the cut-off low rejoined the westerly wave flow at midlatitudes, leaving a wide region of low pressure extending from Africa to Australia. This low-pressure system persisted from September 12–17 and facilitated rapid eastward transport of the biomass burning pollution circulating around both high-pressure systems, as shown for September 14 in Figure 7. By September 18 the pollution reached the South Pacific where it was sampled by the aircraft.

[30] The simulated plume and export pathways are corroborated by column aerosol abundances measured by the Earth Probe Total Ozone Mapping Spectometer (TOMS) satellite; a large aerosol export event from southern Africa to the Indian Ocean took place on September 10–14 [*Chatfield et al.*, 2002; Logan et al., manuscript in preparation, 2000]. The location and timing of the aerosol outflow corresponds quite well with the model enhancements in CO.

[31] Despite biomass burning emissions during 1996 being close to the climatological average [*Olson et al.*, 1999], the meteorological conditions that led to the plume observed over the Pacific on September 18 were anomalous. Figure 8 shows the mean September 1996 surface pressure anomalies relative to the climatology; these anomalies are caused by the September 9–18 period. The low pressure located southwest of the Mascarene High was well developed, allowing efficient outflow from Africa and the South Atlantic. In addition, a sustained area of low pressure extended from Africa to Australia at southern midlatitudes, rather than alternating highs and lows, allowing rapid and uninterrupted westerly transport to the South Pacific. Average September wind speed at 500 hPa over the Indian Ocean was 50–60% greater than the climatology. Indeed, the mean O_3 concentrations observed at 4–12 km altitude by sondes launched from Samoa during September 1996 are 5–10 ppbv higher than the average September O_3 concentrations measured during 1986–1990 and 1995–1999 (long-dashed lines Figure 6).

4.2. Source Regions for CO

[32] In order to identify the contribution of different sources to CO observed above the South Pacific, we conducted a tagged tracer simulation in which CO from different sources was carried as separate tracers [*Bey et al.*, 2001b; *Staudt et al.*, 2001]: (1) biomass burning from South America (180°W–25°W), (2) biomass burning from Africa (25°W–70°E), (3) biomass burning from Australia and Indonesia (70°E–180°E), (4) other anthropogenic sources (fossil fuel and biofuel), and (5) oxidation of CH_4 and isoprene. Biomass burning emissions from Africa and South America are of similar magnitude, as shown in Table 1. Emissions from Indonesia and Australia are a factor of 3 less. Loss of the five CO tracers by reaction with OH is calculated using daily mean OH fields archived from the full chemistry simulation. When the tagged CO fields are summed, the total CO field is identical to that obtained from the full chemistry simulation. The tagged CO run was initialized in mid-July with output from a 1-year run by the Goddard Earth Observing System CHEM (GEOS-CHEM) model [*Bey et al.*, 2001b] with tracers defined in the same way.

[33] Figure 9 shows the column abundance of CO from each source during September. Oxidation of methane and isoprene (not shown) contributes a 40–60% background. Fossil and biofuel emissions account for 14% of Southern Hemispheric CO during September, African biomass burning emissions account for 18%, South American biomass burning emissions account for 10%, and Australian and

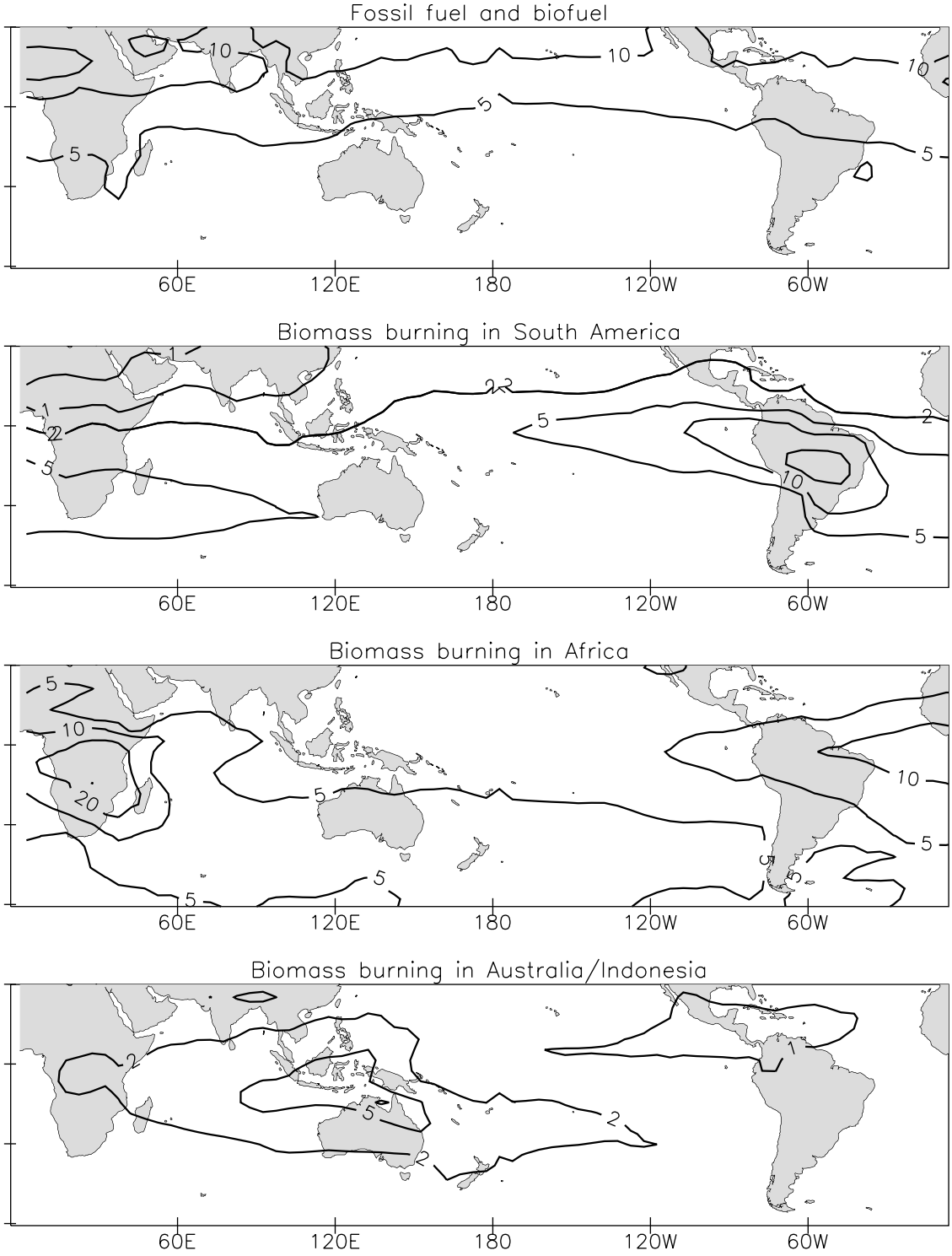

Figure 9. Simulated September mean columns of CO (mol m^{-2}) contributed by fossil and biofuel combustion, biomass burning in South America, biomass burning in Africa, and biomass burning in Australia and Indonesia.

Indonesian biomass burning emissions account for 5%. The large African contribution reflects the early start of the biomass burning season there (June), allowing CO to accumulate by September. The relatively large contribution from fossil and biofuels combustion must reflect, in major part, transport from the Northern Hemisphere as well as emissions in the Southern Hemisphere. Approximately equal amounts of CO above the tropical Pacific (165°E–90°W, 0°–30°S) are contributed by fossil and biofuels (14%), South American biomass burning (13%), and African biomass burning (14%), while burning in Indonesia and Australia contributes much less (5%). The PEM-Tropics A observations did not show obvious signatures from fossil fuel pollution, in contrast to the biomass burning plumes.

Table 2. Concentrations of NO_y Species in the Upper Troposphere Over the South Pacific[a]

Species	DC-8 Observations	Harvard/FSU Model Standard Run	Harvard/FSU Model No Lightning	Harvard/FSU Model No Biomass Burning
NO, pptv	26 (12–56)	22 (16–37)	14 (12–19)	22 (16–36)
NO_x,[b] pptv	34 (15–69)	34 (37–52)	21 (18–25)	33 (26–51)
HNO_3, pptv	58 (24–99)	78 (51–96)	40 (26–55)	74 (48–91)
HNO_3/NO_x, mol mol^{-1}	1.7 (1.2–4.0)	1.9 (1.1–2.6)	1.6 (1.1–2.4)	1.8 (1.0–2.6)
PAN, pptv	40 (23–88)	76 (49–110)	65 (45–96)	51 (34–75)

[a] Median and interquartiles are given for a region defined as 6–12 km, 0°–30°S, 165°E–105°W for the PEM-Tropics A time period of August 28 through October 5, 1996. Statistics in the observations are for the ensemble of the data averaged over HNO_3 measurement intervals. Statistics in the model are for the ensemble of time-averaged concentrations in all grid boxes with the region.

[b] $NO_x = NO + NO_2$.

Since the fossil fuel source is mostly from the Northern Hemisphere, it would presumably contribute an enhancement to the CO background rather than distinct plumes.

5. Sources of NO_x Over the South Pacific

[34] We now turn our attention to the budget of NO_x during PEM-Tropics A. The largest primary sources of NO_x in the Southern Hemisphere during austral spring are biomass burning and lightning (Table 1). The influence of these sources on NO_x concentrations in the South Pacific upper troposphere is shown in Table 2 where model concentrations from the standard simulation are compared to those from simulations with these two primary sources turned off. Lightning has a much larger impact on NO_x concentrations than does biomass burning because of the large source over the western equatorial Pacific and Indonesia (Figure 2). Intense lightning activity was observed in this region during the PEM-Tropics A period [*Fuelberg et al.*, 1999]. With a lifetime ranging from <1 day in the lower troposphere to ~10 days in the upper troposphere, most NO_x from biomass burning that reaches the South Pacific region will have been converted into its reservoir species, PAN and HNO_3. In fact, the simulation without biomass burning has nearly the same NO_x and NO concentrations as in the standard simulation, but PAN concentrations are considerably less. The strong correlation between PAN and CO in the observations (R^2 = 0.78 for 0°–30°S, 165°E–105°W, 6–12 km altitude) and the weak correlation between NO and CO (R^2 = 0.08 for the same region) is consistent with these source attributions in the model. The large contribution to PAN from biomass burning reflects the emission of hydrocarbons together with NO_x from the fires.

[35] Local photochemical model calculations by *Schultz et al.* [1999, 2000] constrained with the ensemble of PEM-Tropics A observations showed that the chemical loss rate (LNO_x) of the expanded NO_x family ($NO_x = NO + NO_2 + NO_3 + 2\ N_2O_5 + HNO_2 + HO_2NO_2$) could be balanced in the lower troposphere by the local chemical production rate (PNO_x) from recycling of PAN (of more importance) and HNO_3 (of lesser importance). Above 6 km altitude, however, LNO_x exceeded PNO_x by a factor ranging from 1.9 (when NO_x loss via N_2O_5 hydrolysis was neglected) to 2.4 (when it was included). Another way to diagnose the chemical imbalance in the NO_x budget is the HNO_3/NO_x concentration ratio. In the upper troposphere most of the imbalance between NO_x sources and sinks results from cycling with HNO_3; thus an accurate simulation of the HNO_3/NO_x ratio indicates that the chemical production and loss rates are properly accounted for in the model. The observed ratio is 1.7 (Table 2), while photochemical steady state models compute the ratio to be 3–5 [*Schultz et al.*, 2000]. The discrepancy between steady state simulated and observed HNO_3/NO_x concentration ratios is consistent with the excess of LNO_x over PNO_x and implies that either primary sources remain important in the NO_x budget of the South Pacific upper troposphere or that our understanding of NO_x chemistry is incomplete.

[36] We investigate the observed chemical imbalance using the Harvard/FSU 3-D model. Median concentrations for the reactive nitrogen species in the model compare well with those observed in the upper troposphere (Table 2). The HNO_3/NO_x ratio of 1.9 in the 3-D model is similar to the observed ratio of 1.7. The 3-D model has a chemical imbalance in the NO_x budget as diagnosed by LNO_x/PNO_x of 1.6, compared to the point model value of 1.9–2.4 as given by *Schultz et al.* [2000]. Because the 3-D model can reproduce both the observed HNO_3/NO_x ratio and the point model chemical imbalance of LNO_x/PNO_x, we conclude that this chemical imbalance is due to transport of primary NO_x into the region rather than to missing chemistry converting HNO_3 to NO_x.

[37] Examination of the NO_x budget terms in the 3-D model for the upper troposphere over the South Pacific (Table 3) gives further insight into the role of transport from primary sources located outside the South Pacific region. The model indicates that 63% of the NO_x source in the South Pacific upper troposphere is due to chemical recycling from the reservoir species HNO_3 and PAN, 28% is due to transport of NO_x into the region, and 9% is due to in situ emissions. Most of the primary NO_x transported into the region in the model is from lightning over the western equatorial Pacific and Indonesia (Figure 2). When lightning sources are turned off in the 3-D model (Table 3), the transport of primary NO_x into the region decreases by more than a factor of 5 and LNO_x/PNO_x is reduced by 50%. The longitudinal gradient of LNO_x/PNO_x in the upper troposphere (Figure 10) supports the importance of westerly transport of this primary source of NO_x; in both the 3-D model and the point model, LNO_x/PNO_x decreases from 3–4 above the western tropical Pacific to 1.3 above the eastern tropical Pacific (with the exception of anomalously high values on flight 8).

[38] *Schultz et al.* [2000] concluded that primary NO_x from lightning was not responsible for the NO_x chemical imbalance in their point model calculations because the greatest imbalances were at low relative humidities, while air masses affected by recent convection have high relative

Table 3. NO_x Budget for Southern Tropical Pacific Upper Troposphere[a]

	Standard Simulation	No Lightning NO_x	No Biomass Burning
	Sources, Mmol day^{-1}		
Net transport into region	15 (28%)	3 (10%)	16 (32%)
Emissions (lightning and aircraft)	5 (9%)	0.4 (2%)	5 (11%)
Total chemical production (PNO_x)	35	24	27
$HNO_3 \rightarrow NO_x$	16 (29%)	7 (27%)	15 (31%)
$PAN \rightarrow NO_x$	18 (34%)	16 (58%)	12 (26%)
Other reactants $\rightarrow NO_x$	1 (2%)	1 (3%)	–
Total sources	55	27	48
	Sinks, Mmol day^{-1}		
Chemical loss (LNO_x)			
$NO_x \rightarrow HNO_3$	36 (67%)	16 (55%)	34 (73%)
$NO_x \rightarrow PAN$	17 (31%)	13 (45%)	11 (25%)
$NO_x \rightarrow$ other products	1 (2%)	–	1.0 (2%)
Total sinks	54	29	46
	Accumulation, Mmol day^{-1}		
Total accumulation	1	−2	2

[a] Budget terms are simulated for the NO_x family (NO_x=NO + NO_2 + NO_3 + 2 N_2O_5 + HNO_2 + HO_2NO_2) averaged for a region defined as 6–12 km, 0–30°S, 165°E–100°W and for the PEM-Tropics A time period (August 28 through October 5, 1996).

humidity [*Cohan et al.*, 1999]. Low relative humidity, however, is consistent with a NO_x source from air masses that have subsided after encountering convection and lightning. Subsidence likely plays an important role in sustaining the chemical imbalance in the NO_x budget. Because the lifetime of NO_x increases with altitude, a primary source at high altitudes will take longer to reach chemical equilibrium. In the tropics, we expect most of the NO_x from lightning to be emitted above the 12-km ceiling of the DC-8 aircraft [*Pickering et al.*, 1998].

[39] We find in the model that transport of primary NO_x from biomass burning makes relatively little contribution to the imbalance in the chemical NO_x budget of the upper troposphere. In fact, as shown in Table 3, turning off biomass burning emissions in the model slightly increases the imbalance. Biomass burning NO_x originates from further away than lightning NO_x, it travels at lower altitudes, and it has a short photochemical lifetime due to the concurrent abundance of hydrocarbons in the fire plumes. All these factors contribute to bringing NO_x from biomass burning into chemical steady state for air masses sampled over the South Pacific.

6. Ozone Budget Over the South Pacific

[40] We now examine the production and loss of O_3 over the South Pacific and how it is affected by emissions from biomass burning and lightning. The mean net production of

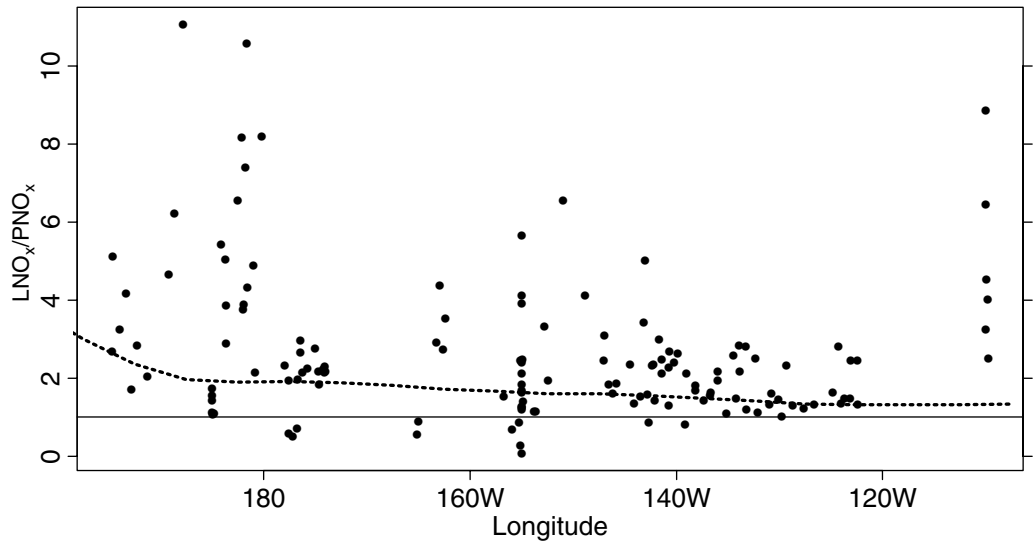

Figure 10. Ratio of 24-hour average NO_x loss to production rates (LNO_x/PNO_x) of the expanded NO_x family (NO_x = NO + NO_2 + NO_3 + 2 N_2O_5 + HNO_2 + HO_2NO_2) computed in a photochemical point model constrained with NO, HNO_3, PAN, and other species observed during PEM-Tropics A [*Schultz et al.*, 2000]. Values for individual points (representing ~3-min averages in the observations) are plotted for 10°–30°S as a function of longitude. Dashed line shows the 3-D model results averaged for 10°–30°S and August 28 through October 5, 1996.

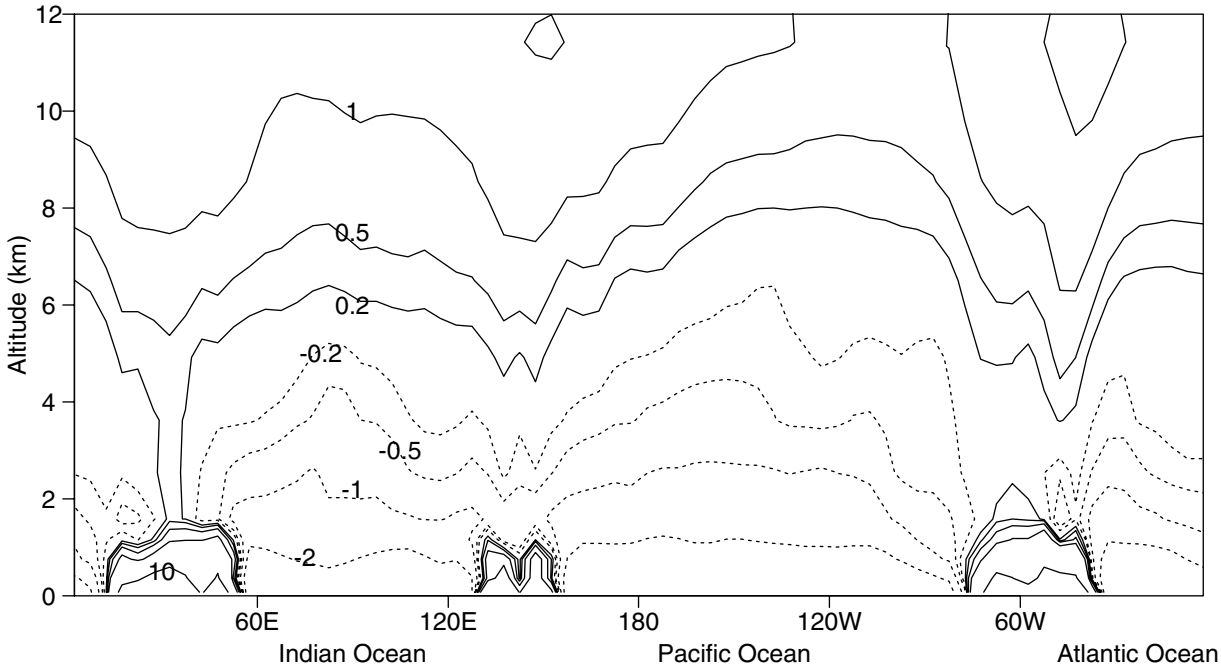

Figure 11. Simulated net production of O_3 (ppbv day^{-1}) averaged over 10°–30°S for the PEM-Tropics A time period (August 28 through October 5, 1996) plotted versus longitude and altitude.

O_3 in the model averaged over the PEM-Tropics A time period is shown in Figure 11. Production and loss rates for the tropical South Pacific, shown in Table 4, are within 20% of values computed by a point photochemical model constrained with in situ observations [*Schultz et al.*, 1999]. The South Pacific troposphere is a region of net photochemical destruction of O_3 with a 0–12-km column loss of 1.5×10^{11} molecules cm^{-2} s^{-1}. Net loss in the marine boundary layer is as high as 3 ppbv day^{-1}. Transition from net loss to net production takes place around 6 km altitude. Net production of up to 2 ppbv day^{-1} is found at 6–12 km over the western Pacific, decreasing to <1 ppbv day^{-1} over the eastern Pacific.

[41] We find that O_3 production is not enhanced in biomass burning plumes as compared to background air masses in the model, reflecting low concentrations of NO_x; there is no significant correlation between simulated CO concentrations and net O_3 production in the middle and upper troposphere over the South Pacific (Figure 12). This finding is consistent with results from point photochemical model calculations (Logan et al., manuscript in preparation, 2000) and implies that the majority of O_3 enhancements from biomass burning in the model are generated in the source regions. Turning off emissions of NO_x from lightning causes a 17% reduction in column O_3 production over the South Pacific, compared to a 14% reduction when biomass burning emissions are turned off. We conclude that simulated tropospheric O_3 production over the South Pacific during PEM-Tropics A has a comparable sensitivity to biomass burning and lightning.

Table 4. Tropospheric O_3 Budget Over the South Pacific During PEM-Tropics A[a]

	P_{O3}	L_{O3}	$(P-L)_{O3}$
	Point Model[b]		
0°–10° S	1.4	3.2	−1.8
10°–30° S	1.8	3.0	−1.2
	Harvard/FSU Model[c]		
0°–10° S	1.8	3.3	−1.5
10°–30° S	2.0	3.5	−1.5

[a] Budget terms (10^{11} molecules cm^{-2} s^{-1}) are calculated for a region defined as 165°E–105°W, 0°–30°S, 0–12 km altitude for the PEM-Tropics A time period of August 28 through October 5, 1996. Gross production rates P_{O3} and gross loss rates L_{O3} are calculated for the odd oxygen family ($O_x = O_3 + O + NO_2 + HNO_4 + 2*NO_3 + 3*N_2O_5 + HNO_3 + PAN + HNO_3$). Considering that O_3 generally accounts for over 90% of O_x, the budgets of O_3 and O_x can be viewed as equivalent. $(P-L)_{O3}$ is the net production rate.

[b] Median values are from *Schultz et al.* [1999].

[c] Average values are given.

7. Summary

[42] We have used a global 3-D model of tropospheric chemistry driven by assimilated meteorological observations to examine the origins of biomass burning pollution plumes observed during PEM-Tropics A and their implications for the regional chemical budgets of NO_x and O_3. Extensive evaluation of model results with aircraft and sonde observations during PEM-Tropics A shows that the model captures major features of biomass burning influence over the South Pacific. It does not capture the layered structure and high CO concentrations of biomass burning plumes observed during PEM-Tropics A, a flaw which we attribute to excessive column mixing during continental deep convection. There is also some indication that the model has insufficient convection to the uppermost troposphere, with implications in particular for subsidence of lightning NO_x over the aircraft flight tracks (ceiling at 12 km altitude). The model reproduces the strong correlation between O_3 and CO observed at

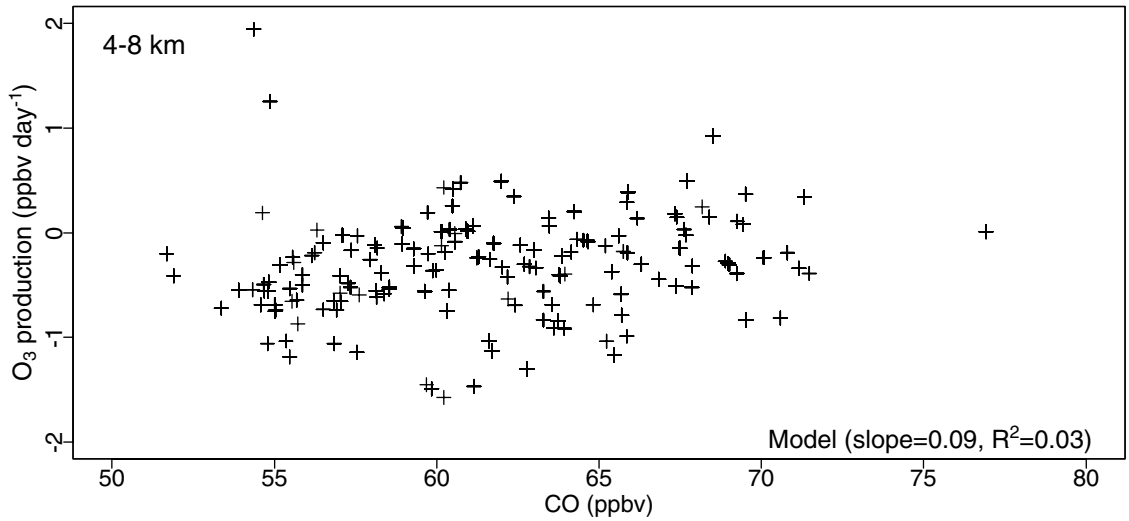

Figure 12. Net production of O_3 (ppbv day^{-1}) plotted versus CO concentration (ppbv) as sampled in the model along the PEM-Tropics A flight tracks for a South Pacific region defined as 10°–30°S, 165°E–105°W, and 4–8 km altitude.

4–8 km over the South Pacific. This correlation illustrates the regional impact of aged biomass burning emissions on the South Pacific troposphere.

[43] The model simulation of biomass burning plumes demonstrates how horizontal advection associated with westerly moving midlatitude cyclones facilitates efficient export of continental- scale air masses from biomass burning source regions and from high-pressure systems located over the South Atlantic and Madagascar. Because of the arrangement of these midlatitude low-pressure systems during September 1996, we find that the South Pacific probably was more heavily influenced by biomass burning pollution than in other years. Indeed, O_3 sonde measurements in the midtroposphere at Samoa in September 1996 were 5–10 ppbv higher than the mean September sonde observations.

[44] A simulation with tagged tracers indicates that 14% of the CO above the tropical South Pacific originated from biomass burning over Africa, 13% originated from biomass burning over South America, 5% originated from biomass burning over Indonesia and Australia, and 14% originated from fossil fuel combustion. Fossil fuel emissions are predominantly located in the Northern Hemisphere and probably contribute to the CO background rather than to distinct plumes. Plumes with an urban origin were not observed during PEM-Tropics A.

[45] Lightning was the most important source of NO_x to the upper troposphere over the South Pacific during PEM-Tropics A, while decomposition of PAN from biomass burning was more important in the lower troposphere. We showed that the previously reported chemical imbalance in the NO_x budget of the upper troposphere can be explained in the 3-D model by subsidence of primary NO_x emitted by lightning over the Indonesian warm pool. Additional chemistry converting HNO_3 to NO_x is not needed in our simulation. When lightning NO_x emissions are turned off in the 3-D model, the ratios of NO_x chemical losses to NO_x chemical sources is decreased by 50%. Emissions of NO_x from biomass burning do not contribute to the chemical imbalance because they originate from further away, are transported in the midtroposphere where the NO_x lifetime is shorter, and are more photochemically active because of concurrent hydrocarbon emissions.

[46] The lower troposphere over the South Pacific is a region of net O_3 destruction, with net loss rates up to 3 ppbv day^{-1}. At ~6 km a transition to net O_3 production takes place, with net production of 1–2 ppbv day^{-1} in the upper troposphere. The net O_3 production in biomass burning plumes is not found to be enhanced relative to the residual background air masses in the model because of low NO_x concentrations in these plumes. Ozone production over the tropical South Pacific is found to have similar sensitivities to biomass burning and lightning emissions.

[47] **Acknowledgments.** This work was supported by the NASA Global Tropospheric Chemistry Program. Amanda Staudt was supported by a National Science Foundation Graduate Fellowship. We would like to express our appreciation to G. Gardner for her help in model development, to M. Prather for the use of an updated chemical transport model driver and Fast-J, and to M. Schultz for point photochemical model results and helpful comments.

References

Balkanski, Y. J., D. J. Jacob, G. M. Gardner, W. C. Graustein, and K. K. Turekian, Transport and residence times of tropospheric aerosols inferred from a global three-dimensional simulation of ^{210}Pb, *J. Geophys. Res.*, *98*, 20,573–20,586, 1993.

Bey, I., D. J. Jacob, R. M. Yantosca, J. A. Logan, B. Field, A. M. Fiore, Q. Li, H. Liu, L. Mickley, and M. Schultz, Global modeling of tropospheric chemistry with assimilated meteorology: Model description and evaluation, *J. Geophys. Res.*, *106*, 23,073–23,095, 2001a.

Bey, I., D. J. Jacob, J. A. Logan, and R. M. Yantosca, Asian chemical outflow to the Pacific in spring: Origins, pathways, and budgets, *J. Geophys. Res.*, *106*, 23,097–23,113, 2001b.

Blake, N. J., et al., Influence of Southern Hemispheric biomass burning on midtropospheric distributions of nonmethane hydrocarbons and selected halocarbons over the remote South Pacific, *J. Geophys. Res.*, *104*, 16,213–16,232, 1999.

Board, A., H. E. Fuelberg, G. L. Gregory, B. G. Heikes, M. G. Schultz, D. R. Blake, J. E. Dibb, S. T. Sandholm, and R. W. Talbot, Chemical characteristics of air from differing source regions during PEM-Tropics A, *J. Geophys. Res.*, *104*, 16,181–16,196, 1999.

Chatfield, R. B., Anomalous HNO_3/NO_x ratio or remote tropospheric air: Conversion of nitric acid to formic acid and NO_x?, *Geophys. Res. Lett.*, *21*, 2705–2708, 1994.

Chatfield, R. B., J. A. Vastano, L. Li, G. W. Sachse, and V. S. Connors, The Great African plume from biomass burning: Generalizations from a three-dimensional study of TRACE A carbon monoxide, *J. Geophys. Res.*, *103*, 28,059–28,078, 1998.

Chatfield, R. W., Z. Guo, G. W. Sachse, D. R. Blake, and N. J. Blake, The subtropical global plume in PEM-T A, PEM-T B, and GASP: How tropical emissions affect the remote Pacific, *J. Geophys. Res.*, *107*, 10.1029/2001JD000497, in press, 2002.

Chin, M., D. J. Jacob, G. M. Gardner, M. S. Foreman-Fowler, P. A. Spiro, and D. L. Savoie, A global three-dimensional model of tropospheric sulfate, *J. Geophys. Res.*, *101*, 18,667–18,690, 1996.

Cohan, D. S., M. G. Schultz, D. J. Jacob, B. G. Heikes, and D. R. Blake, Convective injection and photochemical decay of peroxides in the tropical upper troposphere: Methyl iodide as a tracer of marine convection, *J. Geophys. Res.*, *104*, 5717–5724, 1999.

Diab, R. D., M. R. Jury, J. Combrink, and F. Sokolic, A comparison of anticyclone and trough influences on the vertical distribution of ozone and meteorological conditions during SAFARI-92, *J. Geophys. Res.*, *101*, 23,809–23,822, 1996.

Dibb, J., R. W. Talbot, E. M. Scheuer, D. R. Blake, N. J. Blake, G. L. Gregory, G. W. Sachse, and D. C. Thornton, Aerosol chemical composition and distribution during PEM-Tropics, *J. Geophys. Res.*, *104*, 5785–5800, 1999a.

Dibb, J., R. W. Talbot, L. D. Meeker, E. M. Scheuer, N. J. Blake, D. R. Blake, G. L. Gregory, and G. W. Sachse, Constraints on the age and dilution of Pacific Exploratory Mission-Tropics biomass burning plumes from the natural radionuclide tracer ^{210}Pb, *J. Geophys. Res.*, *104*, 16,233–16,241, 1999b.

Fan, S.-M., D. J. Jacob, D. L. Mauzerall, J. D. Bradshaw, S. T. Sandholm, D. R. Blake, H. B. Singh, R. W. Talbot, G. L. Gregory, and G. W. Sachse, Origin of tropospheric NO_x over subarctic eastern Canada in summer, *J. Geophys. Res.*, *99*, 16,867–16,877, 1994.

Fenn, M., et al., Ozone and aerosol distributions and air mass characteristics over the South Pacific during the burning season, *J. Geophys. Res.*, *104*, 16,197–16,212, 1999.

Fishman, J., J. M. Hoell Jr., R. D. Bendura, R. J. McNeal, and V. W. J. H. Kirchhoff, NASA GTE TRACE A experiment (September–October 1992): Overview, *J. Geophys. Res.*, *101*, 23,865–23,879, 1996a.

Fishman, J., V. G. Brackett, E. V. Browell, and W. B. Grant, Tropospheric ozone derived from TOMS/SBUV measurements during TRACE A, *J. Geophys. Res.*, *101*, 24,069–24,082, 1996b.

Fuelberg, H. E., R. E. Newell, S. P. Longmore, Y. Zhu, D. J. Westberg, E. V. Browell, D. R. Blake, G. L. Gregory, and G. W. Sachse, A meteorological overview of the Pacific Exploratory Mission (PEM) Tropics period, *J. Geophys. Res.*, *104*, 5585–5622, 1999.

Gairola, R. M., and T. N. Krishnamurti, Rain rates based on SSM/I, OLR and raingauge data sets, *Meteorol. Atmos. Phys.*, *50*, 165–174, 1992.

Garstang, M., P. D. Tyson, R. Swap, M. Edwards, P. Kallberg, and J. A. Lindesay, Horizontal and vertical transport of air over southern Africa, *J. Geophys. Res.*, *101*, 23,721–23,736, 1996.

Gregory, G. L., et al., Chemical characteristics of Pacific tropospheric air in the region of the ITCZ and SPCZ, *J. Geophys. Res.*, *104*, 5677–5696, 1999.

Hao, W. M., and M.-H. Liu, Spatial and temporal distribution of tropical biomass burning, *Global Biogeochem. Cycles*, *8*(4), 495–503, 1994.

Hauglustaine, D. A., B. A. Ridley, S. Solomon, P. G. Hess, and S. Madronich, HNO_3/NO_x ratio in the remote troposphere during MLOPEX 2: Evidence for nitric acid reduction on carbonaceous aerosols, *Geophys. Res. Lett.*, *23*, 2609–2612, 1996.

Hoell, J. M., D. D. Davis, D. J. Jacob, M. O. Rodgers, R. E. Newell, H. E. Fuelberg, R. J. McNeal, J. L. Raper, and R. J. Bendura, Pacific Exploratory Mission in the tropical Pacific: PEM Tropics A, August–September 1996, *J. Geophys. Res.*, *104*, 5567–5584, 1999.

Horowitz, L. W., and D. J. Jacob, Global impact of fossil fuel combustion on atmospheric NO_x, *J. Geophys. Res.*, *104*, 23,823–23,840, 1999.

Horowitz, L. W., J. Y. Liang, G. M. Gardner, and D. J. Jacob, Export of reactive nitrogen from North America during summertime, *J. Geophys. Res.*, *103*, 13,435–13,450, 1998.

Hsu, L., M. Schultz, and D. J. Jacob, Methyl iodide: Suitability as a marine atmospheric tracer (abstract), *EOS Trans. AGU*, *80*(17), Spring Meet. Suppl., S76, 1999.

Huntrieser, H., H. Schlager, C. Feigl, and H. Holler, Transport and production of NO_x in electrified thunderstorms: Survey of previous studies and new observations at midlatitudes, *J. Geophys. Res.*, *103*, 28,247–28,264, 1998.

Jacob, D. J., Heterogeneous chemistry and tropospheric ozone, *Atmos. Environ.*, *34*, 2131–2159, 2000.

Jacob, D. J., and M. J. Prather, Radon-222 as a test of convective transport in a general circulation model, *Tellus, Ser. B*, *42*, 118–134, 1990.

Jacob, D. J., et al., Simulation of summertime ozone over North America, *J. Geophys. Res.*, *98*, 14,797–14,816, 1993.

Jacob, D. J., et al., Evaluation and intercomparison of global atmospheric transport models using ^{222}Rn and other short-lived tracers, *J. Geophys. Res.*, *102*, 5953–5970, 1997.

Jacobson, M. Z., and R. P. Turco, SMVGEAR: A sparse-matrix, vectorized gear code for atmospheric models, *Atmos. Environ.*, *28*, 273–284, 1994.

Krishnamurti, T. N., S. Low-Nam, and T. Pasch, Cumulus parameterization and rainfall rates II, *Mon. Weather Rev.*, *111*, 815–828, 1983.

Krishnamurti, T. N., D. K. Oosterhof, and N. Dignon, Hurricane prediction with a high resolution global model, *Mon. Weather Rev.*, *117*, 631–669, 1989.

Krishnamurti, T. N., H. E. Fuelberg, M. C. Sinha, D. Oosterhof, E. L. Bensman, and V. B. Kumar, The meteorological environment of the tropospheric ozone maximum over the tropical South Atlantic, *J. Geophys. Res.*, *98*, 10,621–10,641, 1993.

Krishnamurti, T. N., M. C. Sinha, M. Kanamitsu, D. Oosterhof, H. E. Fuelberg, R. Chatfield, D. J. Jacob, and J. A. Logan, Passive tracer transport relevant to the TRACE-A experiment, *J. Geophys. Res.*, *101*, 23,889–23,907, 1996.

Lary, D. J., A. M. Lee, R. Toumi, M. J. Newchurch, M. Pirre, and J. B. Renard, Carbon aerosols and atmospheric photochemistry, *J. Geophys. Res.*, *102*, 3671–3682, 1997.

Lin, X., M. Trainer, and S. C. Liu, On the nonlinearity of the tropospheric ozone production, *J. Geophys. Res.*, *93*, 15,879–15,888, 1988.

Liu, H., D. J. Jacob, I. Bey, and R. M. Yantosca, Constraints from ^{210}Pb and ^{7}Be on wet deposition and transport in a global three-dimensional chemical tracer model driven by assimilated meteorological fields, *J. Geophys. Res.*, *107*, 12,109–12,128, 2001.

Logan, J. A., An analysis of ozonesonde data for the troposphere: Recommendations for testing 3-D models and development of a gridded climatology for tropospheric ozone, *J. Geophys. Res.*, *104*, 16,115–16,149, 1999.

Mahowald, N. M., P. J. Rasch, and R. G. Prinn, Cumulus parameterization in chemical transport models, *J. Geophys. Res.*, *100*, 26,173–26,189, 1995.

Mauzerall, D. L., J. A. Logan, D. J. Jacob, B. E. Anderson, D. R. Blake, J. D. Bradshaw, B. Heikes, G. W. Sachse, H. B. Singh, and R. W. Talbot, Photochemistry in biomass burning plumes and implications for tropospheric ozone over the tropical South Atlantic, *J. Geophys. Res.*, *103*, 8401–8423, 1998.

Olson, J. R., B. A. Baum, D. R. Cahoon, and J. H. Crawford, Frequency and distribution of forest, savanna, and crop fires over tropical regions during PEM-Tropics A, *J. Geophys. Res.*, *104*, 5865–5876, 1999.

Pickering, K. E., et al., Convective transport of biomass burning emissions over Brazil during TRACE A, *J. Geophys. Res.*, *101*, 23,993–24,012, 1996.

Pickering, K. E., Y. Wang, W.-K. Tao, C. Price, and J.-F. Muller, Vertical distributions of lightning NO_x for use in regional and global chemical transport models, *J. Geophys. Res.*, *103*, 31,203–31,216, 1998.

Portmann, R. W., S. S. Brown, T. Gierczak, R. K. Talukdar, J. B. Burkholder, and A. R. Ravishankara, Role of nitrogen oxides in the stratosphere: A reevaluation based on laboratory studies, *Geophys. Res. Lett.*, *26*, 2387–2390, 1999.

Prather, M., Numerical advection by conservation of second-order moments, *J. Geophys. Res.*, *91*, 6671–6681, 1986.

Prather, M. J., and D. J. Jacob, A persistent imbalance in HO_x and NO_x photochemistry of the upper troposphere driven by deep tropical convection, *Geophys. Res. Lett.*, *24*, 3189–3192, 1997.

Price, C., and D. Rind, A simple lightning parameterization for calculating global lightning distributions, *J. Geophys. Res.*, *97*, 9919–9933, 1992.

Roehl, C. M., J. B. Burkholder, G. K. Moortgat, A. R. Ravishankara, and P. J. Crutzen, Temperature dependence of UV absorption cross sections and atmospheric implications of several alkyl iodides, *J. Geophys. Res.*, *102*, 12,819–12,829, 1997.

Schultz, M. G., et al., On the origin of tropospheric ozone and NO_x over the tropical South Pacific, *J. Geophys. Res.*, *104*, 5829–5844, 1999.

Schultz, M. G., D. J. Jacob, J. D. Bradshaw, S. T. Sandholm, J. E. Dibb, R. W. Talbot, and H. B. Singh, Chemical NO_x budget in the upper troposphere over the tropical South Pacific, *J. Geophys. Res.*, *105*, 6669–6679, 2000.

Singh, H. B., et al., Biomass burning influences on the composition of the remote South Pacific troposphere: Analysis based on observations from PEM-Tropics A, *Atmos. Environ.*, *34*, 635–644, 2000.

Slingo, J. M., The development and verification of a cloud prediction scheme for the ECMWF model, *Q. J. R. Meteorol. Soc.*, *113*, 899–927, 1987.

Staudt, A. C., D. J. Jacob, J. A. Logan, D. Bachiochi, T. N. Krishnamurti, and G. W. Sachse, Continental sources, transoceanic transport, and inter-

hemispheric exchange of carbon monoxide over the Pacific, *J. Geophys. Res.*, *106*, 32,571–32,589, 2001.

Talbot, R. W., J. E. Dibb, E. M. Scheuer, D. R. Blake, N. J. Blake, G. L. Gregory, G. W. Sachse, J. D. Bradshaw, S. T. Sandholm, and H. B. Singh, Influence of biomass combustion emissions on the distribution of acidic trace gases over the South Pacific basin during austral springtime, *J. Geophys. Res.*, *104*, 5623–5634, 1999.

Thompson, A. M., K. E. Pickering, D. P. McNamara, M. R. Schoeberl, R. D. Hudson, J. H. Kim, E. V. Browell, V. W. J. H. Kirchoff, and D. Nganga, Where did tropospheric ozone over southern Africa and the tropical Atlantic come from in October 1992? Insights from TOMS, GTE TRACE A, and SAFARI 1992, *J. Geophys. Res.*, *101*, 24,251–24,278, 1996.

Tyson, P. D., M. Garstang, R. Swap, P. Kallberg, and M. Edwards, An air transport climatology for subtropical southern Africa, *Int. J. Climatol.*, *16*(3), 265–291, 1996.

Wang, Y., D. J. Jacob, and J. A. Logan, Global simulation of tropospheric O_3-NO_x-hydrocarbon chemistry, 1, Model formulation, *J. Geophys. Res.*, *103*, 10,713–10,726, 1998.

Wild, O., and M. J. Prather, Excitation of the primary tropospheric chemical mode in a global three-dimensional model, *J. Geophys. Res.*, *105*, 24,647–24,660, 2000.

Wild, O., Z. Xin, and M. J. Prather, Fast-J: Accurate simulation of in- and below-cloud photolysis in tropospheric chemical models, *J. Atmos. Chem.*, *37*, 245–282, 2000.

D. Bachiochi and T. N. Krishnamurti, Department of Meteorology, Florida State University, 423 Love Building, Tallahassee, FL 32306, USA. (tnk@io.met.fsu.edu)

D. J. Jacob, J. A. Logan, and A. C. Staudt, Division of Engineering and Applied Sciences and Department of Earth and Planetary Sciences, Harvard University, Pierce Hall, 29 Oxford St., Cambridge, MA 02138, USA. (djj@io.harvard.edu; jal@io.harvard.edu; acs@io.harvard.edu)

N. Poisson, Agence de l'Environnement et de la Maitrise de L'Energie, Paris, France.

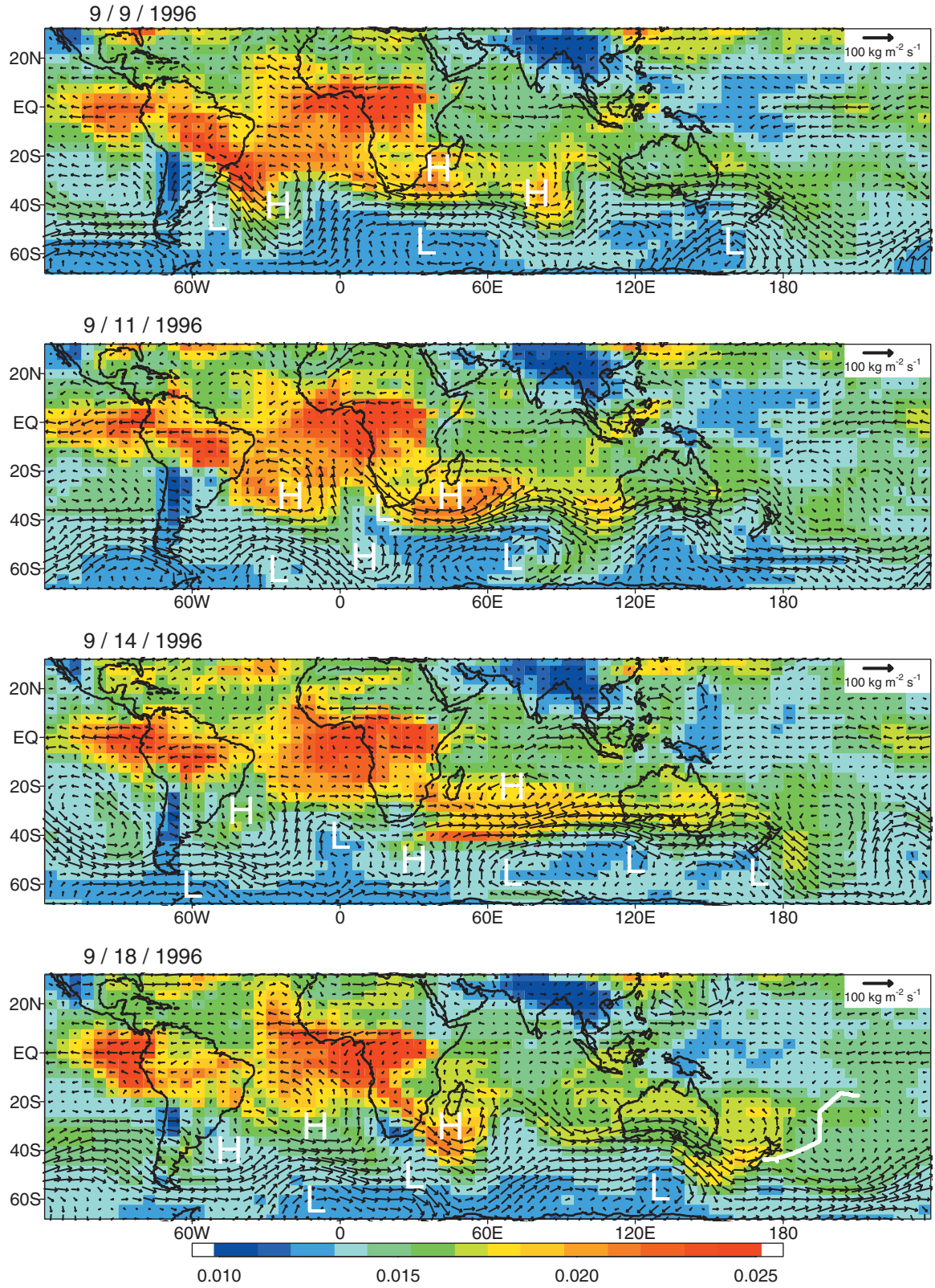

Figure 7. Simulated column CO above the boundary layer (700–85 hPa) in mol m^{-2} for 4 days leading up to the large biomass burning plume event observed between Tahiti and Christchurch, New Zealand, on September 18, 1996. Also shown are the corresponding daily mean centers of high and low surface pressure and air mass flux vectors at 500 hPa.